Chemistry and Materials

The Center for Science Innovation

Research Article

Chem. Mater. 4 (1) 2025, 24-33

Synthesis of α-Fe_2O_3 and α-Fe_2O_3/SiO_2 Composite from Geothermal Waste by Sol-Gel Method and Their Characterization

Rinda Mulmeyda*, Reinardo Ramawijaya Widakusuma, Sabrina Putri Chaerani, Agus Purwanto, Rifqi Almusawi Rafsanjani, Habib Muhammad Zapar, Bagaskoro Pranata Ardhi

Cipta Mikro Material, Bogor, West Java 16340, Indonesia

*Corresponding author: mulmeyda.12@gmail.com

Received
18 January 2025

Received in revised form
19 February 2025

Accepted
24 February 2025

Published online
28 February 2025

DOI
https://doi.org/10.56425/cma.v4i1.91

Abstract

Iron oxide materials, especially hematite (α-Fe_2O_3), have many important applications. Improving the characteristics and physical properties of hematite has been widely developed, one of which is to combine it as a composite structure with porous materials such as silica (SiO_2) as α-Fe_2O_3/SiO_2 composite. This research aims to synthesize α-Fe_2O_3 particles and α-Fe_2O_3/SiO_2 composites. The α-Fe_2O_3/SiO_2 composite was successfully synthesized by using geothermal waste as an alternative source of silica prepared by the sol-gel method. Both synthesized samples were characterized by X-ray diffraction, scanning electron microscopy equipped with energy dispersive spectroscopy, and X-ray fluorescence techniques. The results showed that silica composites on hematite structure slightly affect the morphology, color, or particle size compared to α-Fe_2O_3.

Keywords: hematite, silica, sol-gel, geothermal waste

1. Introduction

Nanotechnology is a modern approach in material engineering that enables the manipulation and design of materials at the nanometer scale, typically ranging from 1 to 100 nm [1]. Nanoparticles, a subset of nanotechnology, hold considerable promise for a wide range of applications due to their distinctive characteristics and benefits, including their optical, electronic, magnetic, and physicochemical properties, which differ significantly from those of bulk materials [2]. Recently, iron oxide nanoparticles have garnered significant attention due to their exceptional thermodynamic properties, pronounced environmental toxicity, resistance to biological toxicity and corrosion, high stability, strong redox potential, and absorption capacity [3,4]. Conventional applications of iron oxide include use in gas sensors, catalysts, fine ceramics, electrodes, magnetic materials, photocatalytic activity, red pigments, and anti-corrosion protective paints [5].

Iron oxide (Fe_2O_3) is a conventional semiconductor that exhibits a negative temperature coefficient of resistance. This material exists in multiple phases, including hematite (α-Fe_2O_3), magnetite (Fe_3O_4), akageneite (β-Fe_2O_3), and maghemite (γ-Fe_2O_3) [6–8]. Two polymorphic forms Fe_2O_3 are recognized, namely the cubic (γ)-phase maghemite and the rhombohedral (α)-hematite [9]. The α-phase is widely regarded as the most significant polymorph, manifesting as hematite with a rhombohedral-centered hexagonal structure and a compact oxygen lattice [10]. α-Fe_2O_3 regarded as the most stable form of Fe_2O_3, is a semiconducting material that exhibits environmental sustainability due to its low band gap energy, E_g = 2.1 eV [11]. This material has found extensive application in various fields due to its numerous advantages, including its low cost, low toxicity, wide variety of colors, and high corrosion resistance [12]. Some notable examples of its use include catalysis, sensors, pigments, lithium-ion batteries, and wastewater treatment.

Bare magnetic nanoparticles, including α-Fe_2O_3, are generally unable to form stable aqueous colloidal suspensions and elemental particles oxidize rapidly, so protection or stabilization methods are needed [13]. One alternative approach is using physical encapsulation, whereby nanoparticles are synthesized in or on porous solid support [14,15]. Among the available porous materials, silica structures are particularly appealing due to their high surface area, uniform pore size, and thermal stability [16,17]. Previous research by Lubis et al. [18]

demonstrated that the catalytic activity of the α-Fe_2O_3/SiO_2 composite is higher than that of bare α-Fe_2O_3. Another study by Sultan et al. [19] showed that the α-Fe_2O_3/SiO_2 composite has the ability of pigment resistance to acid, alkali, thermal, and long-term UV radiation compared to pure α-Fe_2O_3. Another advantage of SiO_2-doped Fe_2O_3 nanoparticles was reported by Arshad et al. [20] who showed promising efficiency for the degradation of Rh B dye, which can be used for the treatment of dyes in wastewater.

Since the properties of materials at the nanometer scale are highly dependent on morphology, size distribution, and conditions during the experiment, it is necessary to determine the most appropriate synthesis method to obtain materials with the expected properties [21]. Some common synthesis methods for Fe_2O_3 nanoparticles include co-precipitation [22], sol-gel [23], hydrothermal [23], pulsed laser ablation [24], and microemulsion [25]. Among the many nanoparticle preparation methods, sol-gel is a widely used method due to the use of small amounts of low-cost precursors, low temperatures, and simple synthesis techniques [26]. The sol-gel method is also a commonly used method for the synthesis of α-Fe_2O_3/SiO_2 composites due to its effectiveness in dispersing small metal and oxide particles in a non-metallic matrix [27-29].

Silica source is one of the factors considered with respect to potential cost-effective and sustainable applications. The most widely known silicas are tetraethyl orthosilicate and tetramethyl orthosilicate, but both are relatively expensive, difficult to obtain, and not environmentally friendly [30]. Previous studies have successfully synthesized α-Fe_2O_3/SiO_2 composites using silica sources derived from natural materials such as rice husks [18,31,32]. However, no one has used geothermal waste as an alternative silica feedstock for the synthesis of α-Fe_2O_3/SiO_2 composites.

This study presents the synthesis of α-Fe_2O_3 and α-Fe_2O_3/SiO_2 composites via a sol-gel method. A novel approach is proposed for the facile and cost-effective fabrication of hematite-silica composite materials. Notably, silica derived from geothermal waste was utilized as an alternative, low-cost, and environmentally sustainable source of silica. This research contributes to the advancement of hematite materials for diverse applications and demonstrates the potential for sustainability-driven innovation through the valorization of industrial byproducts.

2. Materials and Method

2.1 Materials

The materials employed in this study encompass iron (III) chloride ($FeCl_3$, ≥98%, Merck), sodium hydroxide (NaOH, ≥98%, Merck), and silica (SiO_2) derived from the purification of geothermal waste from PT. Geodipa Energi Dieng Indonesia, and distilled water.

2.2 Methods

2.2.1 Silica purification

The pre-treatment before purification consists of washing the geothermal waste with deionized water under continuous stirring. After washing, the solid phase was separated from the filtrate and dried at 100°C for 24 hours before being sieved at 150 µmesh.

A total of 20 g of pre-treated geothermal waste powder dissolved in 800 mL of 1.5 M NaOH solution. The mixture was heated at 90°C for an hour under vigorous stirring. This process yields a brown sodium silicate filtrate, which is separated from its residue by vacuum filtration to eliminate any contaminants. The filtrate undergoes careful titration with 10% HCl while stirred moderately until achieving a neutral pH and the gel formed. The resulting white gel was aged 24 hours and dried at 125°C. After cooling to room temperature, the solid was finely crushed and washed 4 times in 800 mL of distilled water.

2.2.2 Synthesis of Hematite

A total of 16.25 grams of $FeCl_3$ and 12 grams of NaOH were weighed and then dissolved in 50 mL of distilled water ($FeCl_3$:NaOH concentration ratio is 1:3). The homogeneously dissolved $FeCl_3$ solution was then slowly poured into a beaker containing NaOH solution while stirring and heated at 50°C with a magnetic stirrer until the mixture formed a paste-like gel. The gel-like sample was then oven to 200°C for 2 hours. The dried sample was then crushed with a mortar and pestle and the powder sample was washed with distilled water using a Buchner funnel. The washed sample was again oven-dried at 200°C for 2 hours and then crushed again. The sample was then calcined in a furnace at 500°C for 6 hours.

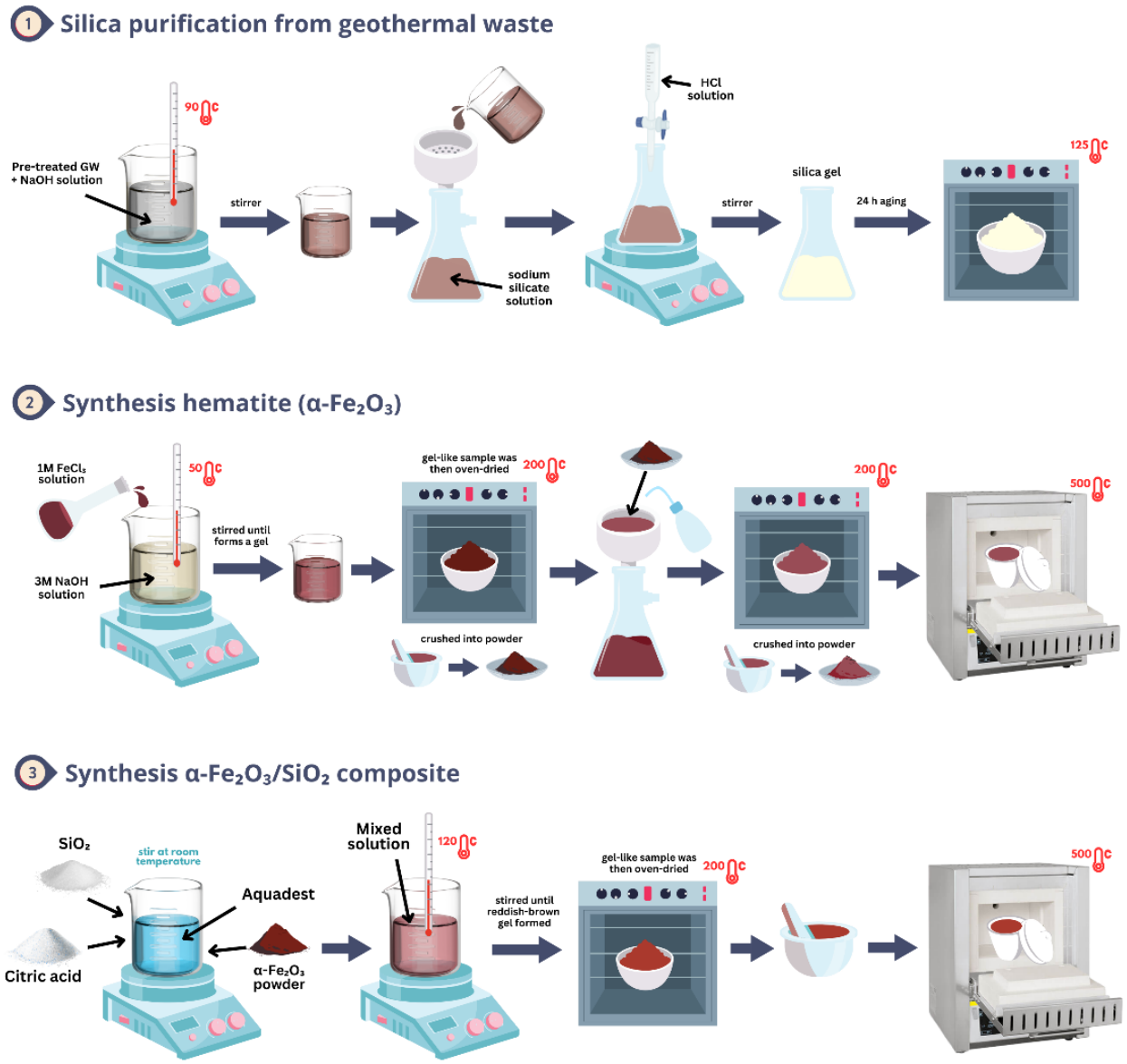

Figure 1. Schematic synthesis procedure of α-Fe_2O_3 and α-Fe_2O_3/SiO_2.

2.2.3 Hematite-silica composite synthesize

The Fe_2O_3 powder obtained from the previous synthesis weighed as much as 3.69 grams. This powder was then mixed with 15.76 grams of citric acid and 1.5 grams of SiO_2 from geothermal waste purification (ratio of 1:1:3). The mixture was dissolved in 50 mL of distilled water and stirred at room temperature for 3 hours. Subsequently, the mixture was subjected to heating at 120°C using a hotplate stirrer, with stirring continued, until a gel-like consistency was achieved. The gel-like sample was then oven-dried at 200°C. The dried sample was then crushed with a mortar and pestle into powder. The sample was then calcined in an oven at 500°C for 6 hours and then characterized.

2.2.4 Characterization method

The synthesized samples were then subjected to a range of characterization techniques to obtain comprehensive information regarding the physical properties of the material. Phase analysis was performed using an X-ray diffractometer (XRD, Malvern PANalytical Aeris). The diffraction pattern results were then analyzed using PANalytical Highscore Plus with references obtained from the ICDD database to identify the phase formed in the sample.

The elemental composition of the samples was subsequently analyzed using the energy-dispersive X-ray

fluorescence (ED-XRF, Malvern PANalytical Epsilon 4) instrument, a tool capable of providing quantitative insights into the elemental composition of materials across the percent to ppm scale. To obtain information on the morphology of the surface structure, particle size, elemental distribution, and local composition of the sample, characterization was performed using scanning electron microscopy equipped with energy dispersive spectroscopy (SEM-EDS, Thermoscientific with resolution a3.0 nm at 30 kV in high vacuum).

3. Results and Discussion

The hematite synthesis was executed through the implementation of the sol-gel method. In this method the process entails the formation of inorganic compounds through chemical reactions in solution at low temperatures, resulting in a phase change from a colloidal suspension (sol) to a gel phase [33]. The sol-gel process encompasses distinct stages, including hydrolysis, condensation, aging, and drying [34]. The technique relies on the hydrolysis and condensation of metal alkoxides or salts to form sol, which then undergo gelation and calcination to produce hematite nanoparticles [35,36]. Through the judicious manipulation of parameters such as precursor chemistry, solvent composition, and drying conditions, the sol-gel method can effectively control the size, surface area, and crystallinity of the materials [37]. It is acknowledged that the formation of nanoparticles encompasses nucleation and crystal growth steps. Among the crystal growth mechanisms, diffusion-based crystal growth, also known as Ostwald ripening, is a notable process. Ostwald ripening is defined as a particle growth mechanism based on dissolution-precipitation in solution [38].

In this study, $FeCl_3.6H_2O$ was utilized as the Fe^{3+} precursor, while NaOH was employed as the precipitation agent. The initial stage of nucleation occurs in the first step, and precipitation is obtained when the amount of $FeCl_3.6H_2O$ and NaOH solution reaches stoichiometric conditions, as depicted by the following equation [21].

$$FeCl_3{\cdot}6H_2O_{(aq)} + 3NaOH_{(aq)} \rightarrow Fe(OH)_{3(s)} + 3NaCl_{(aq)} + 6H_2O_{(l)} \quad (1)$$

$$Fe(OH)_{3(s)} \rightarrow FeOOH_{(s)} + H_2O_{(l)} \quad (2)$$

$$2FeOOH_{(s)}\,(\textit{heating}) \rightarrow Fe_2O_{3(s)} + H_2O_{(l)} \quad (3)$$

The presence of Fe^{3+} ions at a pH 6 has been observed to result in the precipitation of $Fe(OH)_3$ compounds [39]. In this study, the addition of NaOH led to the formation of a reddish-brown precipitate. Based on Equations (1) and (2), it can be deduced that the precipitation obtained in the initial stage of hematite nanoparticle synthesis is FeOOH, also known as goethite. Subsequent to this initial phase, the decomposition of two molecules of goethite (FeOOH) occurs, resulting in the formation of one molecule of Fe_2O_3 and one molecule of H_2O. The thermodynamic properties of FeOOH indicate that the spontaneous decomposition reaction occurs at a temperature of 83°C. However, the reaction rate is accelerated at temperatures ranging from 100 °C to 300 °C [40].

Hematite samples formed from the synthesis results are used for further synthesis with SiO_2 and $C_6H_8O_7$ which dissolves Fe_2O_3 and acts as a Fe^{3+} ion chelator. According to Kunarti et al. [41], in acidic conditions, the oxygen atoms of Si-OH or Si-OR will undergo protonation, resulting in the formation of good leaving groups, such as water or alcohol. This process leads to a decrease in the electron density of the central Si atom, rendering it more electrophilic and more susceptible to hydrolysis or condensation. During hydrolysis and condensation, Fe^{3+} ions from Fe_2O_3 will undergo polymerization, a process facilitated by the deprotonation of coordinated water molecules and hydroxyl groups, as depicted the equation (4) and (5) [42].

$$[Fe(OH)_2^+]_n + Fe^{3+} + 2H_2O \rightarrow [Fe(OH)_2^+]_{n+1} + 2H^+ \quad (4)$$

$$[Fe(OH)_2^+]_n \rightarrow [FeO(OH)]_n + H_n^+ \quad (5)$$

Furthermore, iron (III) precursor ions are trapped and incorporated into the silica gel phase matrix, where they are homogeneously dispersed in the silica gelation process. This condensation causes the mixture to transition to a gel phase, and after drying, it forms xerogel [41]. This theory agrees with the experimental conditions. After reacting at room temperature for 3 hours with stirring and then heating the mixture to 120°C with simultaneous stirring, the hematite and silica mixture quickly turn into a gel and then forms a dry xerogel. In the reaction, citric acid functioned as a chelating agent or complex builder with Fe^{3+}. The presence of three carboxylic groups and one hydroxyl group in citric acid enables the binding of metal cations, thereby forming bonding complexes that exhibit reduced solubility [43]. The citric acid environment fosters the dissolution of the iron(II) oxide phase, which is characterized by its high stability and low solubility. The interaction of citric acid with underlying minerals modifies the mineral's surface characteristics, thereby altering their interaction with other solutes and affecting their dissolution in solution [35,44].

Figure 2 shows images of the α-Fe_2O_3 powder and the α-Fe_2O_3/SiO_2 composite samples. Both samples show a red color, but the α-Fe_2O_3/SiO_2 composite sample has a slightly lighter red color. This shows that the addition of SiO_2 to the α-Fe_2O_3/SiO_2 composite structure does not significantly affect the color of hematite, which is also consistent with the research conducted by Kim et al. [45] that silica-coated

hematite has a CIE Lab measurement value that is almost the same as α-Fe_2O_3, which means that silica has no significant effect on the red color tonality. Similarly, research by Hosseini-Zori et al. [46] reported a slight increase in brighter red color in hematite silica.

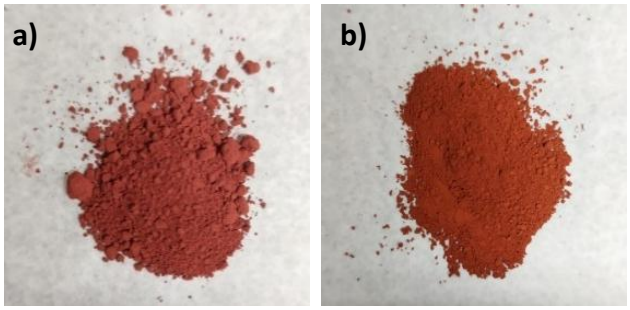

Figure 2. Sample powder a) α-Fe_2O_3 and b) α-Fe_2O_3/SiO_2.

The characterization of the samples was conducted using an XRD instrument, the purpose of which was to identify the phases that had been formed during the synthesis process. The XRD diffraction patterns for the hematite samples are depicted in Fig. 3.

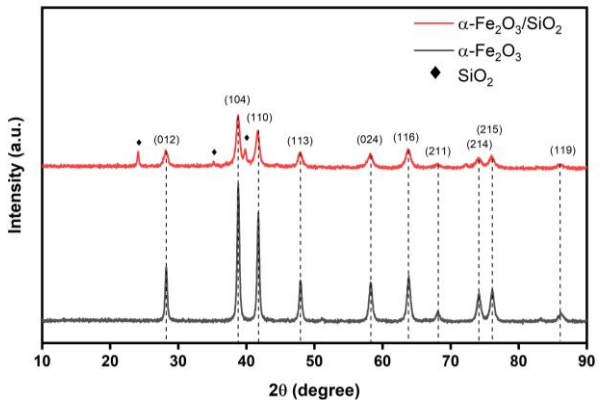

Figure 3. XRD diffraction pattern of Fe_2O_3 and Fe_2O_3/SiO_2.

A thorough analysis of the diffraction patterns reveals the presence of sharp diffraction peaks at specific 2θ values for both samples. These values include 28.09° (012), 38.65° (104), 41.60° (110), 47.79° (113), 58.09° (024), 63.64° (116), 66.24° (211), 73.96° (214), 78.44° (125), and 86.32° (119), which correspond to the standard α-Fe_2O_3 peak based on the ICDD database No. 01-089-0596. There are no other additional peaks in the α-Fe_2O_3 sample, indicating the single phase and high crystal purity of α-Fe_2O_3 synthesized with $FeCl_3.6H_2O$ and NaOH as precursors. In the α-Fe_2O_3/SiO_2 sample, there is another peak which is indicated as the diffraction peak of SiO_2. Based on Fig. 3, it can be seen that both samples have the highest peak intensity in the (104) and (110) fields, indicating that the main characteristic of α-Fe_2O_3 crystals [35]. Based on calculations using the Debye-Scherrer equation, the crystallite size of the α-Fe_2O_3 sample and the α-Fe_2O3/SiO_2 composite were found to be 21.43 nm and 23.81 nm, respectively.

Table 1. Results of XRF analysis on α-Fe_2O_3 and α-Fe_2O_3/SiO_2.

α-Fe_2O_3					
Compound	Fe_2O_3	Cl	P_2O_5	SiO_2	CaO
Conc. unit (%)	97.219	1.754	0.824	-	-
α-Fe_2O_3/SiO_2					
Compound	Fe_2O_3	Cl	P_2O_5	SiO_2	CaO
Conc. unit (%)	87.566	0.704	1.173	10.232	0.325

Based on the XRF characterization results, there are differences in the composition of the constituent elements in the two samples. Of the two samples, Fe_2O_3 is the major element. The percentage of Fe_2O_3 in the α-Fe_2O_3 sample is 97.219%, indicating a high purity hematite phase, while in the α-Fe_2O_3/SiO_2 composite sample, the main composition is α-Fe_2O_3 of 87.566% and SiO_2 of 10.232%. The presence of SiO_2, P_2O_5, and Cl in the first sample is thought to be an impurity found in the initial precursor, $FeCl_3$-$6H_2O$. There are also differences in the composition of the two samples, namely CaO, which was previously absent, but in the second sample, after the addition of silica, there is a CaO component. The same is true for P_2O_5, whose percentage increased slightly compared to before. The presence of CaO and P_2O_5 is thought to be due to SiO_2, which is silica purified from geothermal waste, rather than pure silica. The results of silica purification from geothermal waste show a SiO_2 percentage of 97% and there are still some impurities such as P_2O_5 and CaO.

The elemental composition of both samples was measured by EDS. The results of the quantitative EDS characterization are presented in Table 2.

Table 2. Elemental composition based on EDS measurement.

Element	α-Fe_2O_3		α-Fe_2O_3/SiO_2	
	At%	Wt%	At%	Wt%
Fe	44.6	73.8	26.1	55.4
O	49.5	23.5	47.0	28.5
Si	0.7	0.6	2.3	2.4
Cl	0.4	0.4	0.3	0.4
C	4.8	1.7	19.2	8.8

Based on the EDS measurement results, the dominant elemental composition in both samples is Fe and O. Some trace amounts of elements detected include C, Cl, Na, and Al. It was also observed that a lower percentage of Fe in the α-Fe_2O_3/SiO_2 composite sample compared to the α-Fe_2O_3 sample which is consistent with the XRF composition analysis.

This characterization also provides EDS mapping information showing the distribution of elements as shown in Fig. 4 and Fig. 5. Based on the images of the EDS quantum mapping results on both samples, it can be seen that the Fe and O elements are very evenly distributed, indicating the α-Fe_2O_3 structure that was successfully formed. The image also shows the presence of some impurity components. The presence of Si in the α-Fe_2O_3/SiO_2 composite sample is consistent with the results of XRD phase analysis, which shows the presence of silica phase due to the formation of the α-Fe_2O_3/SiO_2 composite structure.

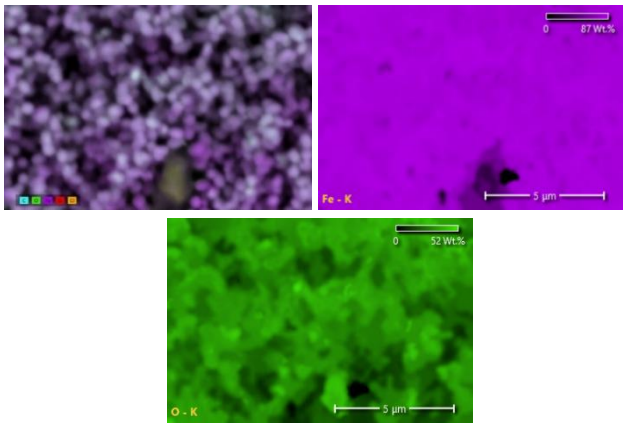

Figure 4. EDS quantum mapping of α-Fe_2O_3 sample.

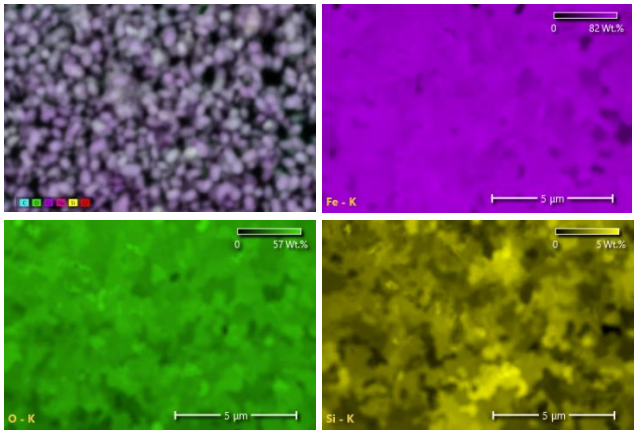

Figure 5. EDS quantum mapping of composite α-Fe_2O_3/SiO_2 sample.

SEM imaging analysis is depicted in Fig. 4 and Fig. 5. This investigation involves the acquisition of SEM images at various magnifications to ensure comprehensive analysis. Figure 6 illustrates the morphology of the α-Fe_2O_3 sample synthesized with $FeCl_3$ and NaOH precursors, resulting in a spherical particle shape. This finding aligns with the research conducted by Nurhayati et al. [21], which demonstrated that α-Fe_2O_3 synthesized with precursors $FeCl_3.6H_2O$ and NaOH exhibits a spherical morphology. Additionally, the research conducted by Lassoued et al. [47], revealed that the synthesis of hematite with various basic reagents, such as NH_4OH, KOH, and NaOH, as precipitation agents, results in spherical particles that resemble a ball shape.

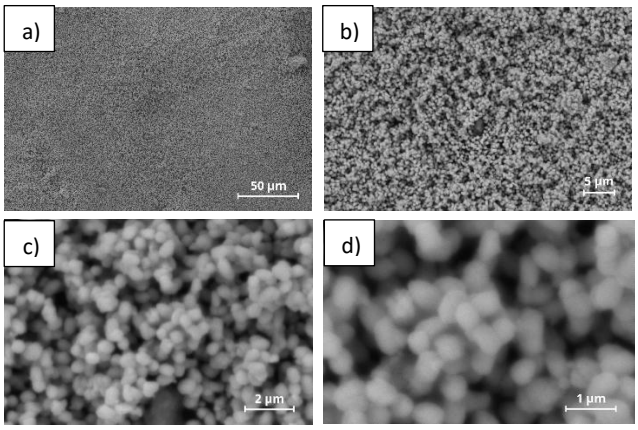

Figure 6. SEM results of a α-Fe_2O_3 at magnification a) 500×, b) 2500×, c) 10.000×, and d) 20.000×.

Hematite obtained by precipitation at neutral or low alkaline pH (<9) is characterized by a spherical particle shape and a wide particle distribution, ranging from 60 to 750 nm, depending on the study [48,49]. At 500× magnification, it can be seen that the particle distribution is uniform. At 20,000× magnification, it can be seen that the α-Fe_2O_3 particles formed have a smooth surface and are almost uniform in size.

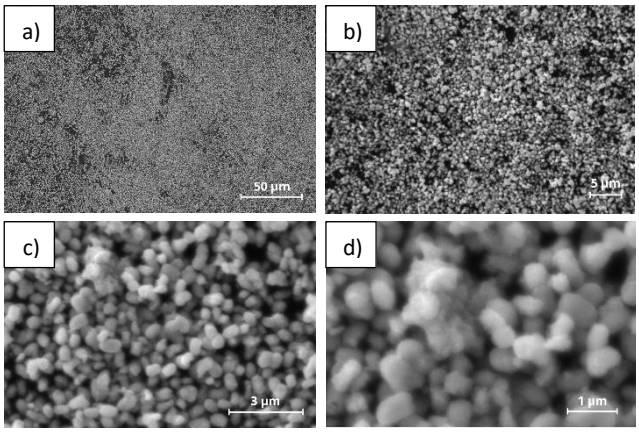

Figure 7. SEM results of a α-Fe_2O_3/SiO_2 at magnification a) 500×, b) 2500×, c) 10.000×, and d) 20.000×.

The morphology of the α-Fe_2O_3/SiO_2 composite sample is shown in Fig. 7, which is almost similar to the morphology of α-Fe_2O_3. In the morphology of the α-Fe_2O_3 sample shown in Fig. 6, the aggregation of α-Fe_2O_3 particles [18]. Meanwhile, the morphology of the α-Fe_2O_3/SiO_2 composite at 500× magnification shows a slight agglomeration of particles at several points, which makes the size and shape of the particles appear non-uniform, which can be seen more clearly at 20,000× magnification. The non-uniform particle size and shape compared to α-Fe_2O_3 may be caused by the bonding of the silica structure with hematite and the strong dipole-dipole interaction between α-Fe_2O_3 nanoparticles and SiO_2 particles [20,50].

The ImageJ software was used for particle analysis. For the sample α-Fe_2O_3, the average particle size was 501.42 nm, while for the sample of composite α-Fe_2O_3/SiO_2 the average particle size was 566.37 nm.

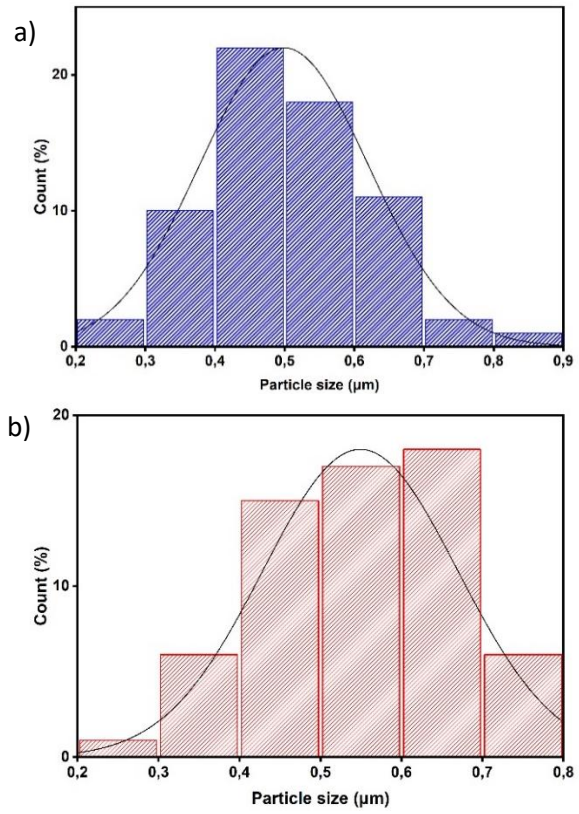

Figure 8. Histograms of particle size distribution a) α-Fe_2O_3 sample and b) α-Fe_2O_3/SiO_2 composite sample.

4. Conclusion

The α-Fe_2O_3/SiO_2 composite was successfully synthesized using geothermal waste as the silica source by the sol-gel method. Silica composites on hematite structure did not significantly affect the morphology, color, or particle size of hematite. Both samples showed a red color, which is the typical color of hematite. The α-Fe_2O_3 particles and α-Fe_2O_3/SiO_2 composite had average particle sizes of 501.42 nm and 566.37 nm, respectively.

Author Contribution

Rinda Mulmeyda: Investigation, Formal analysis, Writing – Original Draft, Visualization. Reinardo Ramawijaya Widakusuma: Visualization, Formal Analysis. Sabrina Putri Chaerani: Investigation, Writing – Review and Editing. Agus Purwanto: Supervision, Project administration, Funding Acquisition. Rifqi Almusawi Rafsanjani: Conceptualization, Methodology, Software, Formal analysis. Habib Muhammad Zapar: Conceptualization, Software, Validation. Bagaskoro Pranata Ardhi: Methodology, Resources.

Conflict of Interest

The authors declare no conflicts of interest regarding the publication of this research.

Acknowledgement

The authors would like to acknowledge the support given by the staff at the PT. Cipta Mikro Material (CMiM), Indonesia for providing the characterization facilities and material for this work.

References

[1] P. Dhull, R.K. Lohchab, M. Kumari, K. Singh, A.K. Bhankhar, . S., A Facile Method for Synthesis of α-Fe2O3 Nanoparticles and Assessment of Their Characterization, *Nature Environment and Pollution Technology*. **23** (2024) 321–330. https://doi.org/10.46488/NEPT.2024.v23i01.027.

[2] N. Baig, I. Kammakakam, W. Falath, Nanomaterials: a review of synthesis methods, properties, recent progress, and challenges, *Mater Adv*. **2** (2021) 1821–1871. https://doi.org/10.1039/D0MA00807A.

[3] S. Attarilar, J. Yang, M. Ebrahimi, Q. Wang, J. Liu, Y. Tang, J. Yang, The Toxicity Phenomenon and the Related Occurrence in Metal and Metal Oxide Nanoparticles: A Brief Review From the Biomedical Perspective, *Front Bioeng Biotechnol*. **8** (2020). https://doi.org/10.3389/fbioe.2020.00822.

[4] N. Malhotra, J.-S. Lee, R.A.D. Liman, J.M.S. Ruallo, O.B. Villaflores, T.-R. Ger, C.-D. Hsiao, Potential Toxicity of Iron Oxide Magnetic Nanoparticles: A Review, *Molecules*. **25** (2020) 3159. https://doi.org/10.3390/molecules25143159.

[5] M. Farahmandjou, F. Soflaee, Synthesis and characterization of α-Fe2O3 nanoparticles by simple co-precipitation method, *Physical Chemistry*

Research. **3** (2015). https://doi.org/10.22036/pcr.2015.9193.

[6] M.I. Dar, S.A. Shivashankar, Single crystalline magnetite, maghemite, and hematite nanoparticles with rich coercivity, *RSC Adv*. **4** (2014). https://doi.org/10.1039/c3ra45457f.

[7] S.I. Andronenko, A.M. Nikolaev, S.M. Suharzhevsky, A.A. Sinelnikov, A.S. Kovalenko, A.G. Ivanova, O.A. Shilova, Phase Composition and Magnetic Properties of Nanoparticles with Magnetite–Maghemite Structure, *Ceramics*. **6** (2023). https://doi.org/10.3390/ceramics6030099.

[8] A.M. Jubb, H.C. Allen, Vibrational spectroscopic characterization of hematite, maghemite, and magnetite thin films produced by vapor deposition, *ACS Appl Mater Interfaces*. **2** (2010). https://doi.org/10.1021/am1004943.

[9] B. Wang, Q. Wei, S. Qu, Synthesis and characterization of uniform and crystalline magnetite nanoparticles via oxidation-precipitation and modified co-precipitation methods, *Int J Electrochem Sci*. **8** (2013). https://doi.org/10.1016/s1452-3981(23)14431-2.

[10] N. Basavegowda, K. Mishra, Y.R. Lee, Synthesis, characterization, and catalytic applications of hematite (α-Fe2O3) nanoparticles as reusable nanocatalyst, *Advances in Natural Sciences: Nanoscience and Nanotechnology*. **8** (2017). https://doi.org/10.1088/2043-6254/aa6885.

[11] G. Cao, Nanostructures and Nanomaterials - Synthesis, Properties and Applications, Imperial Collage Press, London, 2004. https://doi.org/10.1142/9781860945960.

[12] H. Katsuki, E.K. Choi, W.J. Lee, W.S. Cho, K.T. Hwang, W. Huang, S. Komarneni, Controlled synthesis of hexagonal α-Fe2O3 crystals for ceramic colors by hydrothermal reaction of FeCl3 and NaOH solutions, *Ceram Int*. **43** (2017). https://doi.org/10.1016/j.ceramint.2017.07.139.

[13] J. Castillo, V. Vargas, D. Macero, A. Le Beulze, W. Ruiz, B. Bouyssiere, One-step synthesis of SiO2 α−Fe2O3 / Fe3O4 composite nanoparticles with magnetic properties from rice husks, *Physica B Condens Matter*. **605** (2021) 412799. https://doi.org/10.1016/j.physb.2020.412799.

[14] J.-Y. Park, Y.-J. Lee, P.K. Khanna, K.-W. Jun, J.W. Bae, Y.H. Kim, Alumina-supported iron oxide nanoparticles as Fischer–Tropsch catalysts: Effect of particle size of iron oxide, *J Mol Catal A Chem*. **323** (2010) 84–90. https://doi.org/10.1016/j.molcata.2010.03.025.

[15] J.C. Espinosa, C. Catalá, S. Navalón, B. Ferrer, M. Álvaro, H. García, Iron oxide nanoparticles supported on diamond nanoparticles as efficient and stable catalyst for the visible light assisted Fenton reaction, *Appl Catal B*. **226** (2018) 242–251. https://doi.org/10.1016/j.apcatb.2017.12.060.

[16] J. Balbuena, M. Cruz-Yusta, A. Pastor, L. Sánchez, α-Fe2O3/SiO2 composites for the enhanced photocatalytic NO oxidation, *J Alloys Compd*. **735** (2018) 1553–1561. https://doi.org/10.1016/j.jallcom.2017.11.259.

[17] J. Rajagukguk, Fitrilawati, B. Sinaga, J. Kaewkhao, Structural and spectroscopic properties of Er3+ doped sodium lithium borate glasses, *Spectrochim Acta A Mol Biomol Spectrosc*. **223** (2019) 117342. https://doi.org/10.1016/j.saa.2019.117342.

[18] S. Lubis, I. Mustafa, Y. Ermanda, M. Ramadhani, Preparation of SiO_2 /α-Fe_2O_3 Composite from Rice Husk and Iron Sand as a Photocatalyst for Degradation of Acid Black 1 Dye, *J Phys Conf Ser*. **1819** (2021) 012010. https://doi.org/10.1088/1742-6596/1819/1/012010.

[19] S. Sultan, K. Kareem, L. He, Synthesis, characterization and resistant performance of α-Fe2O3@SiO2 composite as pigment protective coatings, *Surf Coat Technol*. **300** (2016) 42–49. https://doi.org/10.1016/j.surfcoat.2016.05.010.

[20] M. Arshad, M. Abbas, S. Ehtisham-ul-Haque, M.A. Farrukh, A. Ali, H. Rizvi, G.A. Soomro, A. Ghaffar, M. Yameen, M. Iqbal, Synthesis and characterization of SiO2 doped Fe2O3 nanoparticles: Photocatalytic and antimicrobial activity evaluation, *J Mol Struct*. **1180** (2019) 244–250. https://doi.org/10.1016/j.molstruc.2018.11.104.

[21] T. Nurhayati, F. Iskandar, M. Abdullah, Khairurrijal, Syntheses of hematite (α-Fe2O3) nanoparticles using microwave-assisted calcination method, in: Materials Science Forum, 2013: pp. 197–203. https://doi.org/https://doi.org/10.4028/www.scientific.net/MSF.737.197.

[22] A. Lassoued, B. Dkhil, A. Gadri, S. Ammar, Control of the shape and size of iron oxide (α-Fe2O3) nanoparticles synthesized through the chemical precipitation method, *Results Phys*. **7** (2017) 3007–3015. https://doi.org/10.1016/j.rinp.2017.07.066.

[23] F. Ozel, H. Kockar, O. Karaagac, Growth of Iron Oxide Nanoparticles by Hydrothermal Process: Effect of Reaction Parameters on the Nanoparticle Size, *J*

Supercond Nov Magn. **28** (2015) 823–829. https://doi.org/10.1007/s10948-014-2707-9.

[24] P. Maneeratanasarn, T. Van Khai, S.Y. Kim, B.G. Choi, K.B. Shim, Synthesis of phase-controlled iron oxide nanoparticles by pulsed laser ablation in different liquid media, *Physica Status Solidi (a)*. **210** (2013) 563–569. https://doi.org/10.1002/pssa.201228427.

[25] K. Kekalo, K. Koo, E. Zeitchick, I. Baker, Microemulsion Synthesis of Iron Core/Iron Oxide Shell Magnetic Nanoparticles and Their Physicochemical Properties, *MRS Proceedings*. **1416** (2012) mrsf11-1416-jj05-54. https://doi.org/10.1557/opl.2012.736.

[26] Z.N. Kayani, S. Arshad, S. Riaz, S. Naseem, Synthesis of Iron Oxide Nanoparticles by Sol-Gel Technique and Their Characterization, *IEEE Trans Magn*. **50** (2014). https://doi.org/10.1109/TMAG.2014.2313763.

[27] F. Tari, M. Shekarriz, S. Zarrinpashne, A. Ruzbehani, Synthesis, characterization, and optimization of α-Fe $_2$ O $_3$ /silica nanocomposites using homogenous precipitation method, *Int J Appl Ceram Technol*. **14** (2017) 810–819. https://doi.org/10.1111/ijac.12684.

[28] W. Ge, X. Zhang, X. Ge, K. Liu, Synthesis of α-Fe2O3/SiO2 nanocomposites for the enhancement of acetone sensing performance, *Mater Res Bull*. **141** (2021) 111379. https://doi.org/10.1016/j.materresbull.2021.111379.

[29] G. Ennas, A. Musinu, G. Piccaluga, D. Zedda, D. Gatteschi, C. Sangregorio, J.L. Stanger, G. Concas, G. Spano, Characterization of Iron Oxide Nanoparticles in an Fe $_2$ O $_3$ −SiO $_2$ Composite Prepared by a Sol−Gel Method, *Chemistry of Materials*. **10** (1998) 495–502. https://doi.org/10.1021/cm970400u.

[30] S. Affandi, H. Setyawan, S. Winardi, A. Purwanto, R. Balgis, A facile method for production of high-purity silica xerogels from bagasse ash, *Advanced Powder Technology*. **20** (2009) 468–472. https://doi.org/10.1016/j.apt.2009.03.008.

[31] S.M. Reda, S.M. Al-Ghannam, S.N. Abd El-Rahman, Effect of Source of Silica on Properties of Fe2O3/SiO2 Nanocompsites and Their Application on Hepatic Injury in Rats as Adsorbents for Removal of Heavy Metal from Drinking Water, *Asian Journal of Chemistry*. **30** (2018) 625–632. https://doi.org/10.14233/ajchem.2018.21062.

[32] A.-T. Vu, T.N. Xuan, C.-H. Lee, Preparation of mesoporous Fe2O3·SiO2 composite from rice husk as an efficient heterogeneous Fenton-like catalyst for degradation of organic dyes, *Journal of Water Process Engineering*. **28** (2019) 169–180. https://doi.org/10.1016/j.jwpe.2019.01.019.

[33] M. Elma, A. Paramita, A. Sumardi, Pengaruh Penambahan Dual Katalis Pada Silica-Carbon Xerogel sebagai Material Pelapis Organo Silica Membranes, *Konversi*. **7** (2018). https://doi.org/10.20527/k.v7i2.6498.

[34] E. Wiyono, F.W. Mahatmanti, S. Priatmoko, Pengaruh Jenis Prekursor dan Suhu Kalsinasi terhadap Karakteristik Komposit TiO2-SiO2 dan Aplikasinya dalam Degradasi Rhodamin B, *Jurnal MIPA UNNES*. **41** (2018).

[35] N. Utari, H. Maulidina, R. Arilasita, H. Widiyandari, Suharno, B. Purnama, Citric acid concentration tune of structural and magnetic properties in hematite (α−Fe2O3) nanoparticles synthesized by sol−gel method, *Mater Res Express*. **10** (2023). https://doi.org/10.1088/2053-1591/acbf0c.

[36] E. Paulson, M. Jothibas, Significance of thermal interfacing in hematite (α-Fe2O3) nanoparticles synthesized by sol-gel method and its characteristics properties, *Surfaces and Interfaces*. **26** (2021). https://doi.org/10.1016/j.surfin.2021.101432.

[37] Jegadeeswari A, Punitha T, Synthesis and characterization of iron Oxide (hematite) nanoparticles by sol-gel method, *Nanoscale Reports*. **3** (2020). https://doi.org/10.26524/nr.3.23.

[38] B. Gilbert, H. Zhang, F. Huang, M.P. Finnegan, G.A. Waychunas, J.F. Banfield, Special phase transformation and crystal growth pathways observed in nanoparticles†, *Geochem Trans*. **4** (2003). https://doi.org/10.1186/1467-4866-4-20.

[39] P. Kurniawan, M. Kasmiyatun, Soebiyono, Reduksi Kandungan Logam Berat Fe Pada Air Sungai Jetis Salatiga Secara Adsorbsi Menggunakan Karbon Aktif, *CHEMTAG Journal of Chemical Engineering*. **1** (2020) 12–17. https://doi.org/https://doi.org/10.56444/cjce.v1i1.1323.

[40] A. Kurniawan, G. Saito, T. Nomura, T. Akiyama, Faster generation of nanoporous hematite ore through dehydration of goethite under vacuum conditions, *ISIJ International*. **61** (2021) 493–497. https://doi.org/https://doi.org/10.2355/isijinternational.ISIJINT-2020-403.

[41] et. al Eka Sri Kunarti, Pengujian Aktivitas Komposit Fe2O3-SiO2 Sebagai Fotokatalis Pada Fotodegradasi 4-Klorofenol, *Manusia Dan Lingkungan. Kimia FMIPA UGM. Yogyakarta*. **16** (2009).

[42] E.G. Rightor, M.S. Tzou, T.J. Pinnavaia, Iron oxide pillared clay with large gallery height: Synthesis and properties as a Fischer-Tropsch catalyst, *J Catal*. **130** (1991). https://doi.org/10.1016/0021-9517(91)90089-M.

[43] H. Han, W. Yin, D. Wang, Z. Zhu, B. Yang, J. Yao, New insights into the dispersion mechanism of citric acid for enhancing the flotation separation of fine siderite from hematite and quartz, *Colloids Surf A Physicochem Eng Asp*. **641** (2022). https://doi.org/10.1016/j.colsurfa.2022.128459.

[44] B. Zinder, G. Furrer, W. Stumm, The coordination chemistry of weathering: II. Dissolution of Fe(III) oxides, *Geochim Cosmochim Acta*. **50** (1986). https://doi.org/10.1016/0016-7037(86)90244-9.

[45] Y. Kim, J.-H. Pee, J.H. Chang, K. Choi, K.J. Kim, D.-Y. Jung, Silica Effect on Coloration of Hematite Nanoparticles for Red Pigments, *Chem Lett*. **38** (2009) 842–843. https://doi.org/10.1246/cl.2009.842.

[46] M. Hosseini-Zori, E. Taheri-Nassaj, A.R. Mirhabibi, Effective factors on synthesis of the hematite–silica red inclusion pigment, *Ceram Int*. **34** (2008) 491-496. https://doi.org/10.1016/j.ceramint.2006.11.012.

[47] A. Lassoued, M.S. Lassoued, B. Dkhil, A. Gadri, S. Ammar, Synthesis, structural, optical and morphological characterization of hematite through the precipitation method: Effect of varying the nature of the base, *J Mol Struct*. **1141** (2017). https://doi.org/https://doi.org/10.1016/j.molstruc.2017.03.077.

[48] S. Zhan, D. Chen, X. Jiao, S. Liu, Facile fabrication of long α-Fe2O3, α-Fe and γ-Fe2O3 hollow fibers using sol–gel combined co-electrospinning technology, *J Colloid Interface Sci*. **308** (2007) 265–270. https://doi.org/https://doi.org/10.1016/j.jcis.2006.12.026.

[49] D. Li, H. Liu, L. Feng, A Review on Advanced FeNi-Based Catalysts for Water Splitting Reaction, *Energy & Fuels*. **34** (2020) 13491–13522. https://doi.org/10.1021/acs.energyfuels.0c03084.

[50] B.C. Ang, I.I. Yaacob, I. Nurdin, Investigation of Fe_2O_3/SiO_2 Nanocomposite by FESEM and TEM, *J Nanomater*. **2013** (2013). https://doi.org/10.1155/2013/980390.